Analysis of the thermal behaviour of the LFI-RAA cryogenic chamber in ALS

TITLE:

DOC. TYPE: TECHNICAL NOTE

PROJECT REF.: PL-LFI-PST-TN-066 **PAGE:** i of IV, 19

ISSUE/REV.: 1.0 **DATE:** September, 23rd 2005

Prepared by	**F. CUTTAIA** **L. STRINGHETTI** **L. TERENZI** **LFI** **Project System Team**	**Date:** **Signature:**	**September 2005**
Checked by	**A. MENNELLA** **G. MORGANTE** **LFI** **Project System Team**	**Date:** **Signature:**	**September 2005**
Agreed by	**C. BUTLER** **LFI** **Program Manager**	**Date:** **Signature:**	**September 2005**
Approved by	**N. MANDOLESI** **LFI** **Principal Investigator**	**Date:** **Signature:**	**September 2005**

DISTRIBUTION LIST

Recipient	Company / Institute	E-mail address	Sent
N. MANDOLESI	IASF/INAF – Sez. Bologna	mandolesi@bo.iasf.cnr.it	Yes
C. BUTLER	IASF/INAF – Sez. Bologna	butler@bo.iasf.cnr.it	Yes
M. BERSANELLI	UniMI – Milano	marco.bersanelli@fisica.unimi.it	Yes
M. TOMASI	CNR – Milano	tomasi@mi.iasf.cnr.it	Yes
M. LAPOLLA	ALENIA SPAZIO – LABEN	lapolla.m@laben.it	Yes
P. LEUTENEGGER	ALENIA SPAZIO – LABEN	Leutenegger.p@laben.it	Yes
C. FRANCESCHET	-	franceschet.c@laben.it	Yes
LFI CALIBRATION TEAM			Yes
			Yes
LFI Local PROGRAM MANAGER			Yes
LFI SPCC	IASF/INAF – Sez. Bologna	lfispcc@bo.iasf.cnr.it	Yes

CHANGE RECORD

Issue	Date	Sheet	Description of Change	Release
Draft	Sept. 2005	All	Draft Issue of the Document	0.1

TABLE OF CONTENTS

TABLE OF CONTENTS ..... **IV**

1 INTRODUCTION AND SCOPE **1**

2 APPLICABLE DOCUMENTS **1**

3 REFERENCE DOCUMENTS **1**

4 DESCRIPTION OF ACQUISITION SYSTEM **1**

5 ANALYSIS OF TEMPERATURE BEHAVIOUR **2**

5.1 SET 1 FROM 17/07/05 (14:26) TO 22/07/05 (23:59) 2
5.2 SET 2 FROM 23/07/05 (00:00) TO 25/07/05 (18:23) 12
5.3 SET 3 WARM-UP OF SKY LOAD 16
5.4 STABILITY OF DATA 18

6 CONCLUSIONS **19**

1 INTRODUCTION AND SCOPE

The scope of this document is to present a thermal analysis of the RAA Cryofacility used in the LFI QM Test in ALS . The data used for this analysis cover 8 days of testing: from the 18th to the 25th of July 2005. The aim of the analysis is to understand the behaviour of the LFI RAA cryogenic chamber and to provide useful indications to fully exploit the cryochamber thermal data during the instrument calibration data analysis.

Commento [L1]: Non sarebbe il caso di dire che al di là del periodo scelto I dati presi per l'analisi sono sostanzialmente I tre casi in cui la RAA e quindi la camera si trovano (troveranno????) durante I test? E cioè il caso con sky a 20 K il caso con Sky a 30 K e il caso di transizione tra I due….

2 APPLICABLE DOCUMENTS

3 REFERENCE DOCUMENTS

4 DESCRIPTION OF ACQUISITION SYSTEM

The cryofacility sensors acquisition software was implemented by CSL in LabView environment. The hardware EGSE is composed by two Lakeshore monitors and a Keithley one. The EGSE is able to read and store up to 34 sensors with a duty cycle of 30 seconds. . At the same time the EGSE is designed to control a set of temperatures inside the chamber: these stages are controlled usinga PI (Proportional and Integrative) feedback loop. In the table below the positions of the sensors inside the chamber are listed and described.

Name	Position	Note
BEU_1	On BEU foot	See Fig. 4
BEU_2	On	See Fig. 4
VG1_1	V- Groove 1, on Cu interface that simulates the V- Groove Connection	
VG1_2	V- Groove 1 See Above	
VG2_1	V- Groove 2	
VG2_2	V- Groove 2	
TT_P1	Thermal Tent on Panel P1 (D1)	
TT_P2	Thermal Tent on Panel P2 (D2)	
TTP32	Thermal Tent on Panel P3b (D3)	
TTP41	Thermal Tent on Panel P4b (D4) First	
TTP42	Thermal Tent on Panel P4b (D5) Second	
TT_P9	Thermal Tent on Panel P9 (D6)	
TTP31	Thermal Tent on Panel P3 (D7)	
TT_41	Thermal Tent on Panel P4 (D8) First	
TT_42	Thermal Tent on Panel P4 (D9) Second	
TTP51	Thermal Tent on Panel P5 (D10)	
TT_P6	Thermal Tent on Panel P6 (D11)	
TT_P7	Thermal Tent on Panel P7 (D12)	
SFt_1	Strut_Feet_1 on FPU foot	
SFt_2	Strut_Feet_2 on FPU foot See Fig.	
SS_F1	Stainless steel Flange, part of cryo-MGSE.	

Name	Position	Note
VG3_1	V- Groove 3	Damaged during cooldown
VG3_2	V- Groove 3	
Sky_1	Aluminium flange that sustains Sky Load	Central Position
Sky_2	Aluminium flange that sustains Sky Load	Central Position
FPU_1	On Copper interface of LR2	
FPU_2	On Copper interface of LR2	
Ref_1	See Fig.	
Ref_2	See Fig.	

Commento [L2]: Facciamo lo scanner delle foto che ci ha passato M. Lapolla?

TABLE 1 SENSOR POSITIONS

5 Analysis of temperature behaviour.

The analysis has been conducted on three sets of data acquired in different conditions:

- Set 1 Sky load at high temperature with a set point of 31.6K
- Set 2 Sky load at low temperature with a set point of 20K
- Set 3 Data acquired during passive warm up of Sky load.

5.1 SET 1 FROM 17/07/05 (14:26) TO 22/07/05 (23:59)

In the Figure 1 is presented the behaviour of 3 basic temperature sensors during the whole acquisition time. All the sensor values were monitored and stored but in the figures below only the Sky Load, Reference Load and FPU are displayed, nevertheless the analysis has been conducted all over the 32 sensors.

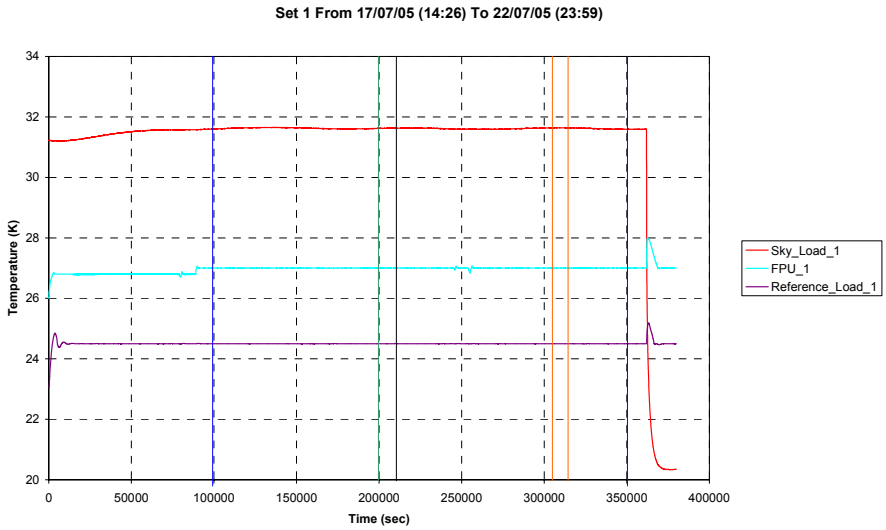

FIG. 1 SET 1 COMPLETE ACQUISITION.

A long time scale analysis was performed on the data contained in the area delimited by the two blue lines in Fig.1. The resulting statistics can be summarized in Table 2, but a first clear result is reported in Fig.2. This figure shows the occasional variability of the acquisition duty cycle with respect to 30 seconds, showing the occurrence of anticipated (29 sec) and delayed (31 sec) acquisition. This inconsistency can affect the FFT analysis that requires a uniform time sampling.

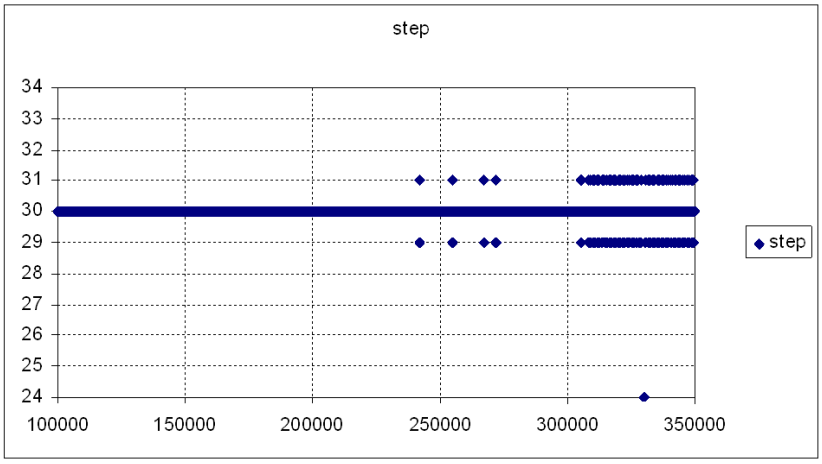

FIG. 2 SAMPLING 30 SEC

	Mean (K)	STD (K)	Min (K)	Max (K)	Ripple (K)
BEU_1	299.910	0.367	298.774	300.676	1.902
BEU_2	293.324	0.016	293.276	293.382	0.105
VG1_1	166.200	0.008	166.160	166.237	0.076
VG1_2	158.851	0.030	158.735	158.933	0.198
VG2_1	106.200	0.011	106.160	106.258	0.098
VG2_2	104.760	0.048	104.651	104.890	0.239
TT_P1	83.194	0.108	83.009	83.383	0.374
TT_P2	84.517	0.115	84.317	84.692	0.376
TTP32	77.853	0.100	77.683	78.014	0.331
TTP41	51.131	0.055	51.033	51.240	0.208
TTP42	54.502	0.061	54.400	54.618	0.218
TT_P9	82.372	0.093	82.218	82.532	0.315
TTP31	77.750	0.101	77.574	77.900	0.326
TT_41	51.234	0.052	51.137	51.303	0.166
TT_42	54.516	0.056	54.411	54.592	0.181
TTP51	79.901	0.106	79.722	80.077	0.356
TT_P6	74.298	0.096	74.141	74.465	0.323
TT_P7	72.433	0.092	72.286	72.597	0.312
SFt_1	24.908	0.006	24.893	24.918	0.025
SFt_2	24.971	0.006	24.957	24.980	0.023
SS_Fl	86.757	1.224	85.332	89.725	4.393
VG3_1	21.495	0.051	21.437	21.946	0.509
VG3_2	58.000	0.007	57.932	58.064	0.132
Sky_1	31.619	0.018	31.586	31.654	0.068
Sky_2	31.686	0.017	31.652	31.720	0.068
FPU_1	26.999	0.009	26.836	27.063	0.227
FPU_2	26.649	0.009	26.482	26.708	0.226
Ref_1	24.500	0.002	24.493	24.507	0.014
Ref_2	24.505	0.002	24.498	24.512	0.014

TABLE 2

COMPLETE STATISTIC ON SET 1

From the table above it is quite evident the high ripple level of BEU_1 and of the SS flange. The low frequency noise in the BEU is found in many other sensors, as it results in the FFT analysis conducted on the same time set.

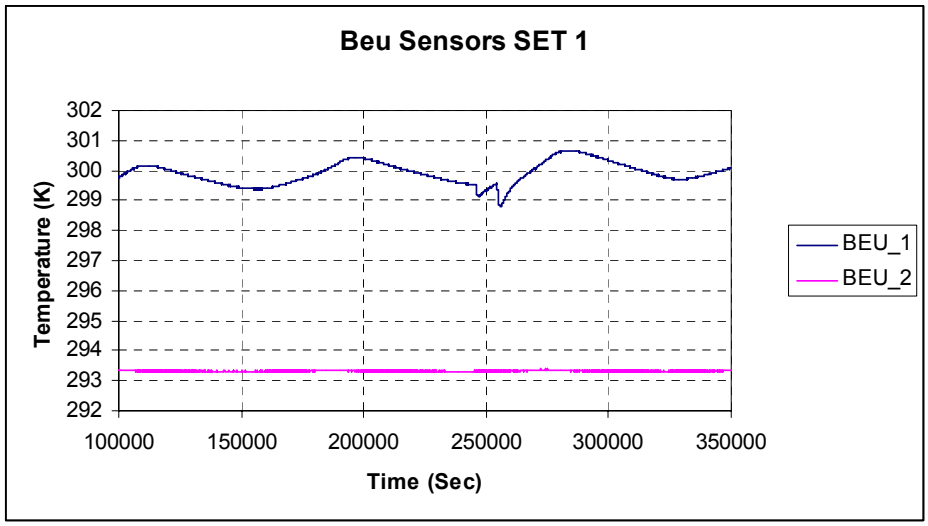

FIG. 3 BEU SENSORS VALUES.

Sensor BEU_1

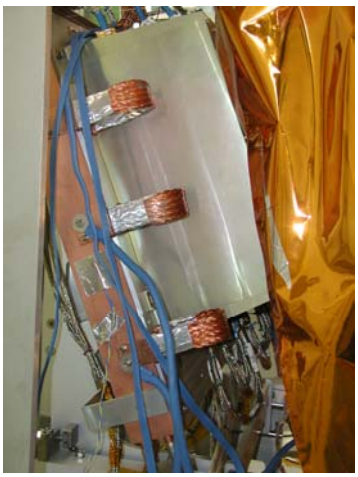

Sensor BEU_2

FIG. 4 BEU SENSORS POSITION ON RAA

The BEU_2 sensor is placed near the temperature controller of the BEU and it shows a level of instability lower by an order of magnitude with respect to the first BEU thermometer.

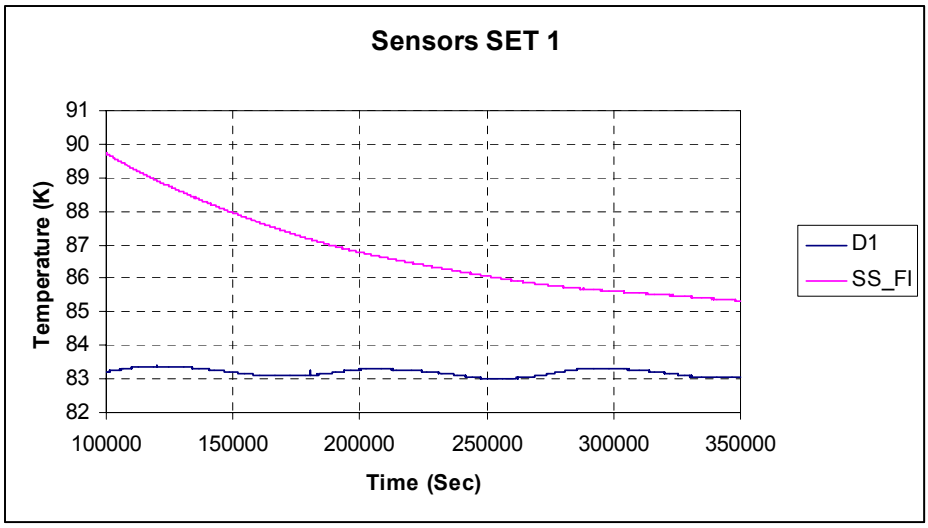

FIG. 5 STAINLESS STEEL FLANGE AND THERMAL TENT ON PANEL 1

From the figure above it is quite evident that, even if the SS flange was not thermalized yet, it does not show a strong correlation with the thermal tent (D1) while it seems to be more correlated with the general decreasing trend of the sky load temperature sensor (see Fig.6)

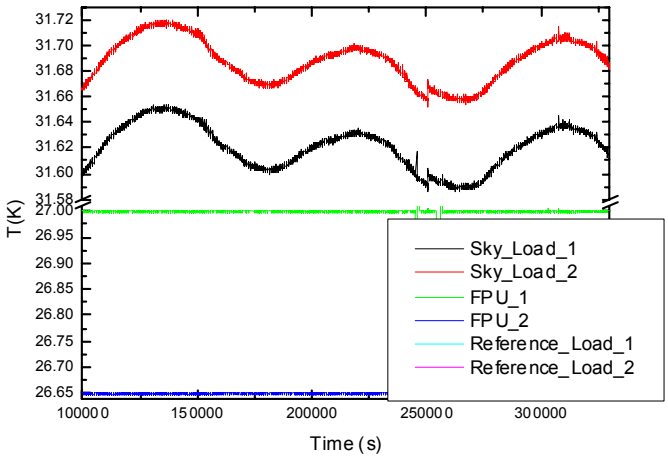

FIG. 6 SKY LOAD AND FPU SENSORS

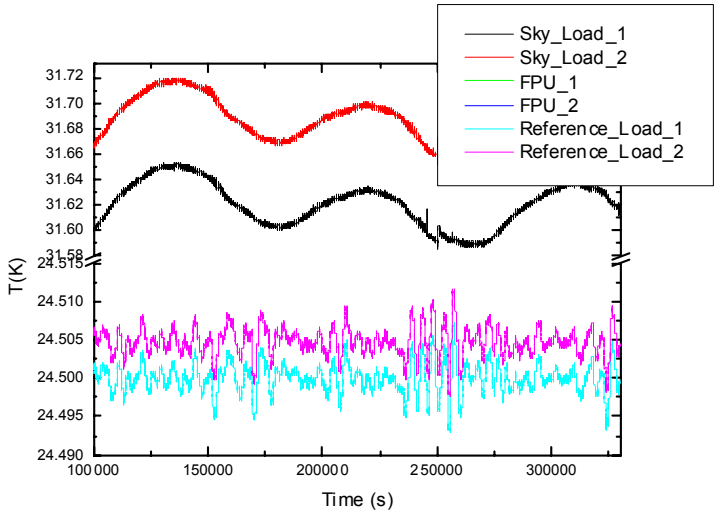

FIG. 7 SKY LOAD AND RL SENSORS

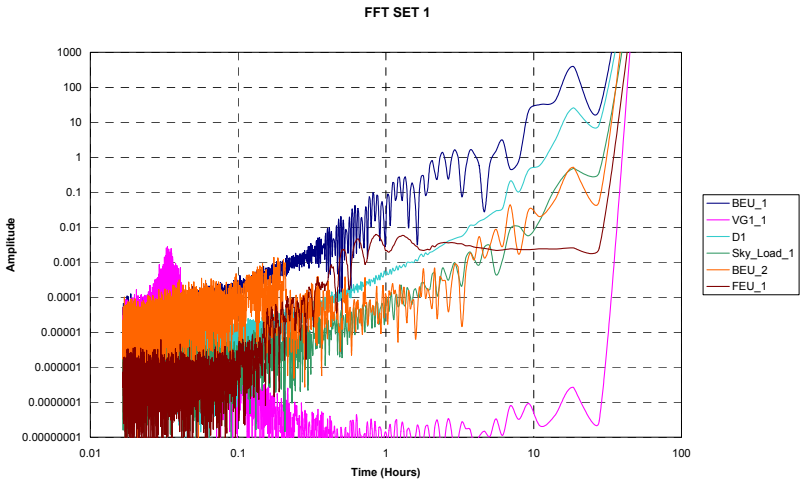

FIG. 8 FAST FOURIER TRANSFORM OF SET 1

In Fig. 8, the presence of a strong component at very low frequency (T=17 hours), is quite clear in the majority of the sensors spectrum. The height of the peak in the BEM_1 thermometer and the phase components indicate that this contribution might have a starting point in the BEU. A more detailed analysis on the time domain data evidenced that this feature is likely to be due to a daily (24 hours) modulation in the

system, driven by environmental fluctuations. Because of time sampling effects and duration of data used in the FFT this modulation footprint peaks around 17 hours.
As it will be shown later on, there is also a strong correlation between the Thermal Tent regions and the Sky Load at higher frequencies. This is the most interesting result from the thermal point of view. In the picture below the FFT of D1 and Sky load is shown.

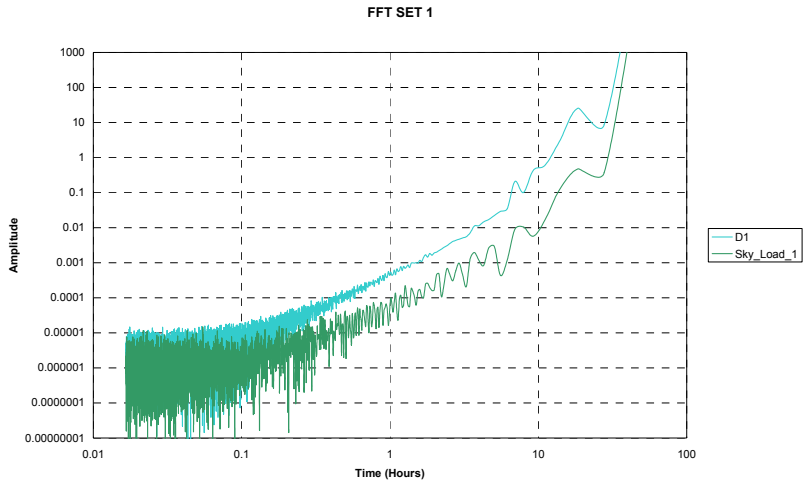

FIG. 9 FFT ANALYSIS OF SKY LOAD AND DI SENSORS.

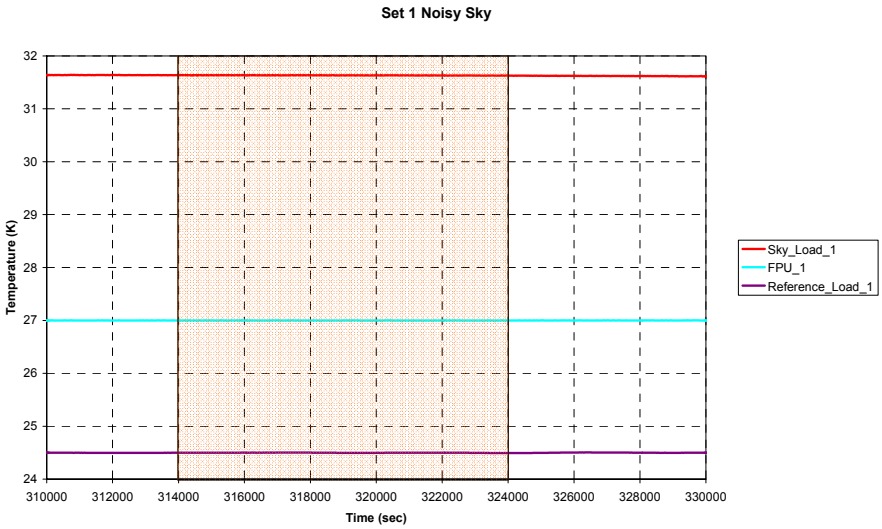

FIG. 10 NOISY SKY SUBSET

Analyzing data at time scales of the order of some hours, another feature is found in Sky Load: in different periods of acquired data, they show different noise spectra.

In Fig. 10 and Fig. 11, the analyses conducted on two significant subsets are presented. The main difference is that the first Sky Load sensor shows a higher noise level than the other. The two sets have an equal time span.
Table 3 and Table 4 summarize some statistics information of all the sensors in the two subsets.

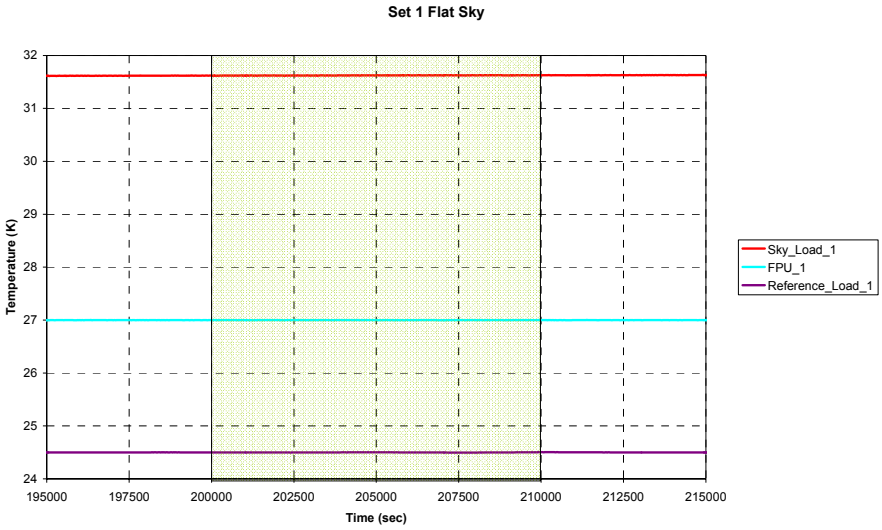

FIG. 11 FLAT SKY SUBSET

.

	Mean (K)	STD (K)	Min (K)	Max (K)	Ripple (K)
BEU_1	299.868	0.067	299.760	299.992	0.232
BEU_2	293.312	0.006	293.292	293.331	0.039
VG1_1	166.200	0.008	166.179	166.221	0.042
VG1_2	158.819	0.014	158.782	158.863	0.080
VG2_1	106.200	0.010	106.170	106.230	0.060
VG2_2	104.787	0.012	104.753	104.820	0.068
TT_P1	83.189	0.026	83.142	83.231	0.089
TT_P2	84.500	0.031	84.447	84.553	0.106
TTP32	77.858	0.027	77.811	77.906	0.094
TTP41	51.147	0.015	51.112	51.169	0.057
TTP42	54.519	0.016	54.483	54.544	0.061
TT_P9	82.413	0.024	82.369	82.454	0.085
TTP31	77.759	0.026	77.713	77.802	0.088
TT_41	51.249	0.016	51.205	51.272	0.066
TT_42	54.532	0.017	54.489	54.554	0.065
TTP51	79.905	0.028	79.856	79.954	0.098
TT_P6	74.328	0.025	74.283	74.371	0.088
TT_P7	72.468	0.024	72.424	72.508	0.084
SFt_1	24.909	0.002	24.903	24.911	0.008
SFt_2	24.971	0.002	24.966	24.973	0.007
SS_FI	85.513	0.016	85.485	85.542	0.058
VG3_1	21.518	0.069	21.479	21.783	0.304
VG3_2	58.000	0.003	57.993	58.008	0.014
Sky_1	31.633	0.002	31.626	31.637	0.011
Sky_2	31.701	0.002	31.695	31.706	0.011
FPU_1	27.000	0.001	26.997	27.003	0.005
FPU_2	26.649	0.001	26.646	26.652	0.006
Ref_1	24.500	0.002	24.493	24.503	0.010
Ref_2	24.504	0.002	24.498	24.507	0.009

TABLE 3 NOISY SKY SUBSET

	Mean (K)	STD (K)	Min (K)	Max (K)	Ripple (K)
BEU_1	300.066	0.064	299.958	300.184	0.226
BEU_2	293.321	0.006	293.303	293.338	0.036
VG1_1	166.200	0.008	166.177	166.222	0.045
VG1_2	158.869	0.012	158.838	158.899	0.061
VG2_1	106.200	0.012	106.168	106.229	0.061
VG2_2	104.760	0.014	104.727	104.798	0.071
TT_P1	83.276	0.009	83.256	83.293	0.037
TT_P2	84.602	0.016	84.574	84.647	0.073
TTP32	77.936	0.012	77.915	77.958	0.044
TTP41	51.178	0.004	51.170	51.187	0.017
TTP42	54.554	0.005	54.544	54.562	0.017
TT_P9	82.456	0.008	82.440	82.470	0.030
TTP31	77.839	0.010	77.820	77.855	0.035
TT_41	51.295	0.003	51.288	51.302	0.014
TT_42	54.581	0.003	54.574	54.587	0.013
TTP51	79.992	0.013	79.968	80.016	0.048
TT_P6	74.392	0.010	74.373	74.408	0.035
TT_P7	72.524	0.008	72.507	72.539	0.033
SFt_1	24.913	0.001	24.912	24.915	0.003
SFt_2	24.976	0.001	24.975	24.978	0.003
SS_FI	86.540	0.043	86.467	86.615	0.148
VG3_1	21.469	0.047	21.451	21.773	0.323
VG3_2	58.000	0.003	57.993	58.010	0.017
Sky_1	31.630	0.002	31.625	31.634	0.009
Sky_2	31.696	0.002	31.692	31.701	0.009
FPU_1	27.000	0.001	26.998	27.002	0.005
FPU_2	26.650	0.001	26.647	26.652	0.005
Ref_1	24.500	0.002	24.498	24.505	0.007
Ref_2	24.505	0.002	24.502	24.510	0.007

TABLE 4 FLAT SKY SUBSET

As already mentioned, it is worth noting that the noisy subset shows higher values of standard deviation for both the sky load sensors and the Thermal Tent sensors.

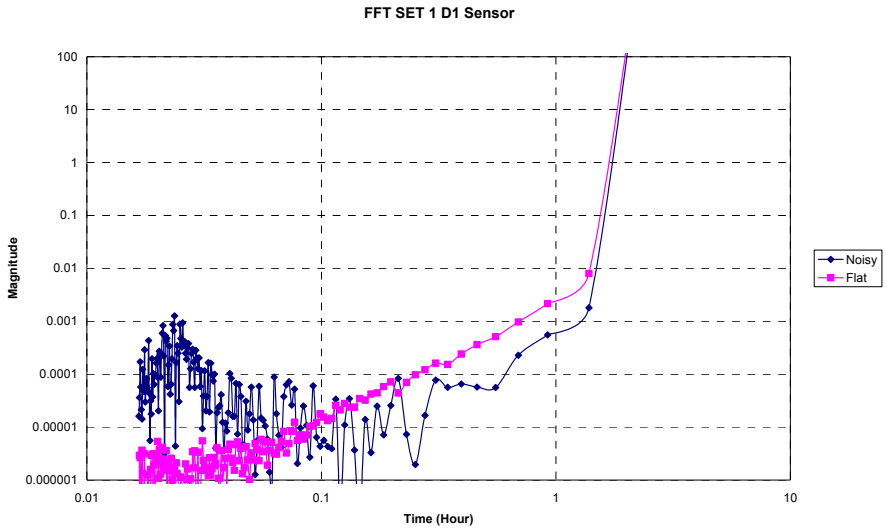

FIG. 12 FFT TRANSFORM OF SENSOR D1 (THERMAL TENT)

Commento [L3]: Non diciamo nulla su questa cosa? Come è possibile? Perché mai ci dovrebbero essere nel tempo due stati così diversi?

5.2 SET 2 FROM 23/07/05 (00:00) TO 25/07/05 (18:23)

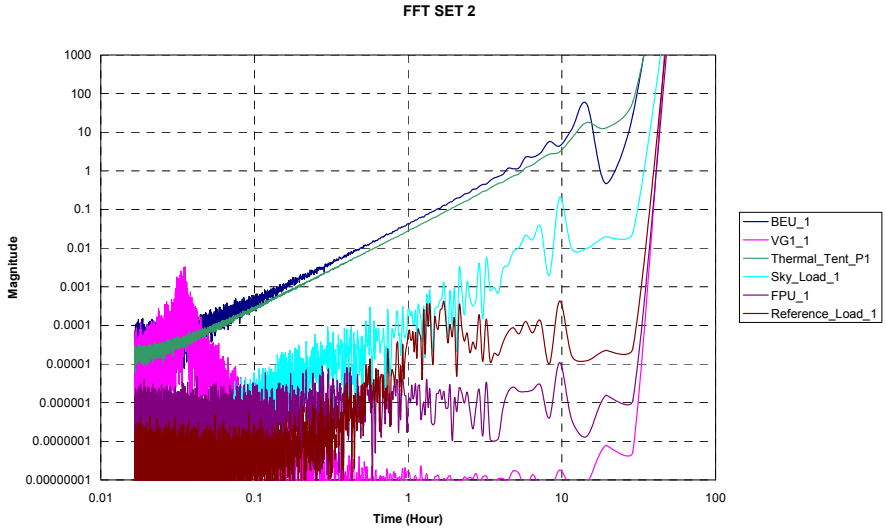

FIG. 13 FFT TRANSFORM OF THE COMPLETE SET 2

	Mean (K)	STD (K)	Min (K)	Max (K)	Ripple (K)
BEU_1	299.839	0.167	299.552	300.115	0.563
BEU_2	293.311	0.009	293.281	293.338	0.057
VG1_1	166.200	0.009	166.171	166.226	0.055
VG1_2	158.826	0.016	158.781	158.876	0.095
VG2_1	106.200	0.011	106.167	106.232	0.066
VG2_2	104.818	0.021	104.768	104.884	0.116
TT_P1	83.051	0.060	82.934	83.137	0.203
TT_P2	84.365	0.075	84.223	84.477	0.254
TTP32	77.728	0.066	77.602	77.827	0.225
TTP41	51.052	0.035	50.990	51.103	0.113
TTP42	54.418	0.040	54.350	54.477	0.127
TT_P9	82.298	0.057	82.187	82.380	0.194
TTP31	77.629	0.061	77.510	77.718	0.208
TT_41	51.166	0.029	51.114	51.208	0.094
TT_42	54.445	0.033	54.385	54.492	0.107
TTP51	79.779	0.071	79.645	79.886	0.240
TT_P6	74.209	0.062	74.092	74.299	0.207
TT_P7	72.355	0.058	72.243	72.442	0.200
SFt_1	24.896	0.003	24.891	24.901	0.010
SFt_2	24.957	0.003	24.952	24.962	0.010
SS_FI	85.167	0.028	85.116	85.215	0.098
VG3_1	21.493	0.042	21.471	21.731	0.260
VG3_2	58.000	0.003	57.991	58.009	0.017
Sky_1	20.350	0.004	20.344	20.364	0.020
Sky_2	20.391	0.004	20.384	20.405	0.020
FPU_1	27.000	0.001	26.998	27.003	0.005
FPU_2	26.649	0.001	26.647	26.651	0.004
Ref_1	24.500	0.001	24.498	24.503	0.005
Ref_2	24.505	0.001	24.503	24.508	0.005

TABLE 5 COMPLETE STATISTIC ON SET 2

In the second set of data, with the Sky Load thermalized at its lower temperature, the statistical analysis show lower values of standard deviation.
In this case the Sky Load is strongly connected to the 20K cooler cold head by means of the dedicated heat switch. This has a double effect: on one side, it reduces the coupling of the sky load with the thermal tent, while on the other hand the sky load results more correlated with Reference Load, FPU and all the stages connected to the 20K cold head. If we compare the correlation factor between the sky load and all these other stages in Set 1 and Set 2, this effect is evident (see Fig. 14 and Fig. 15). In these plots, it clearly results a thermal decoupling between the two BEU sensors; the BEU_1 sensor is strongly linked to Thermal Tent behaviour, while BEU_2 sensor is mainly correlated to the FPU.

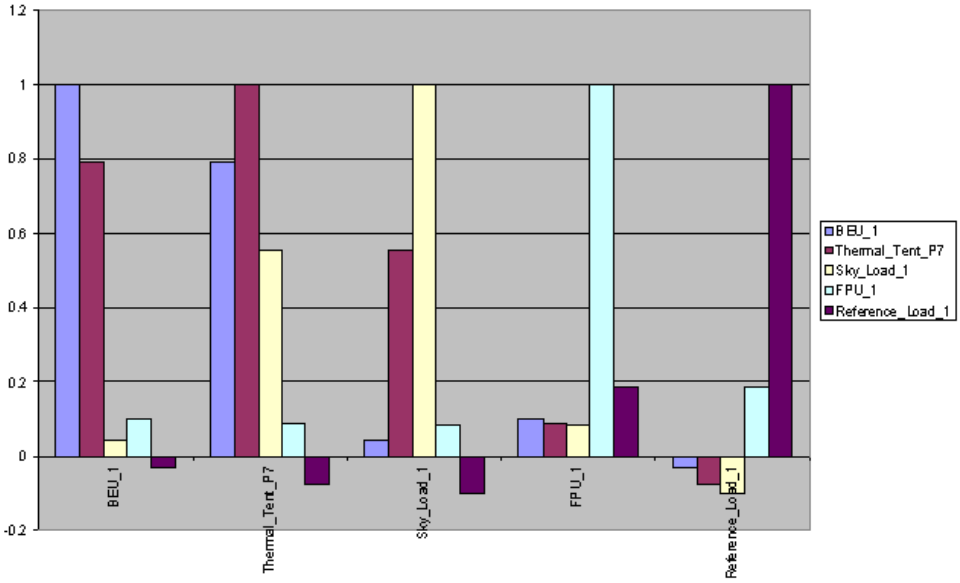

FIG. 14 CORRELATION BETWEEN BEU, THERMAL TENT, SKY LOAD, FPU AND REF LOAD IN SET1

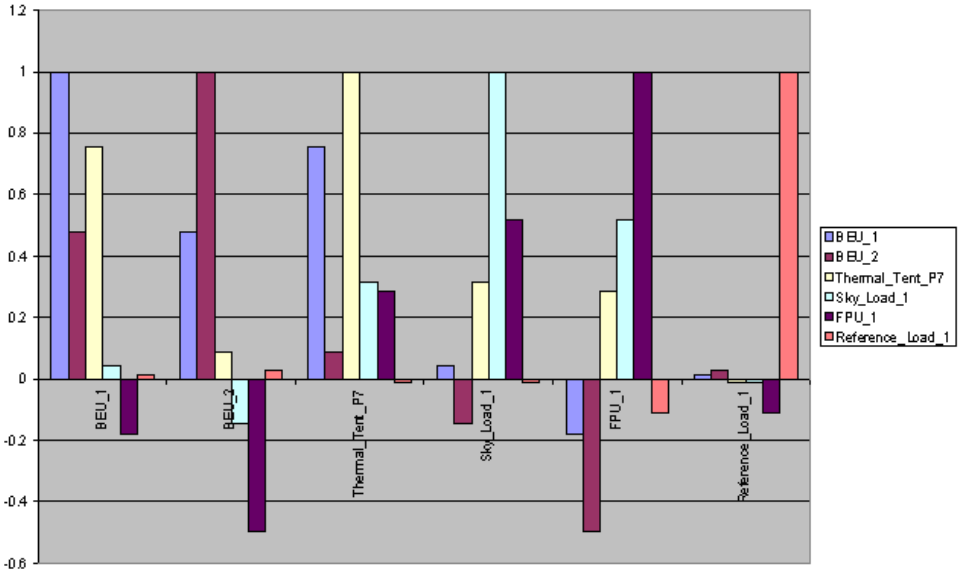

FIG. 15 CORRELATION BETWEEN BEU, THERMAL TENT, SKY LOAD, FPU AND REF LOAD IN SET2

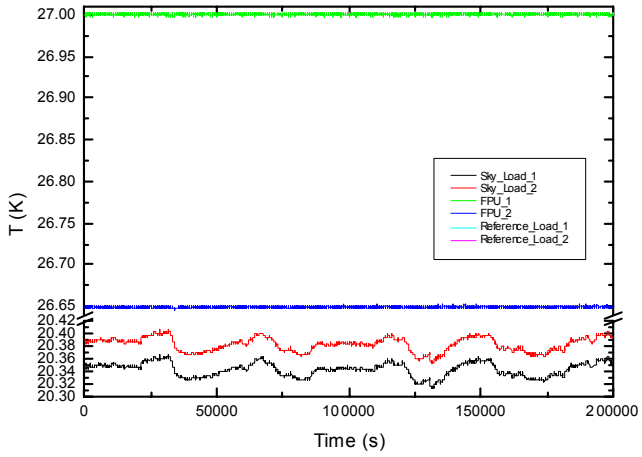

FIG. 16 SKY LOAD AND FPU SENSORS

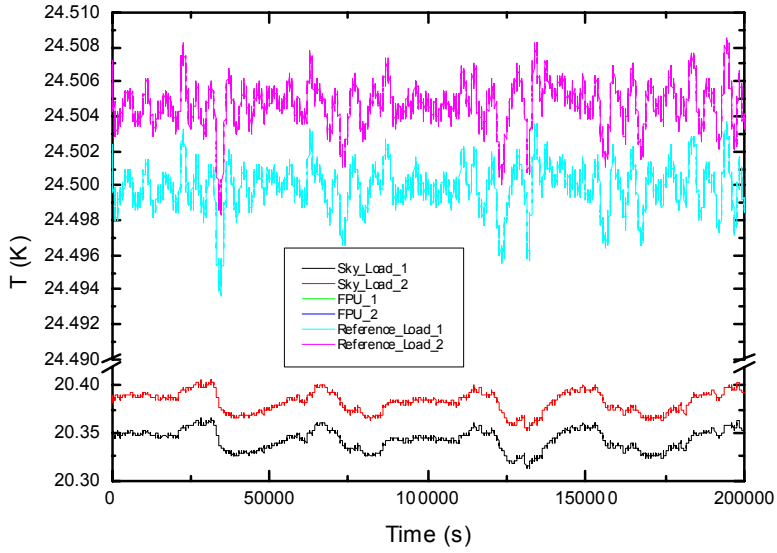

FIG. 17 SKY LOAD AND RL SENSORS

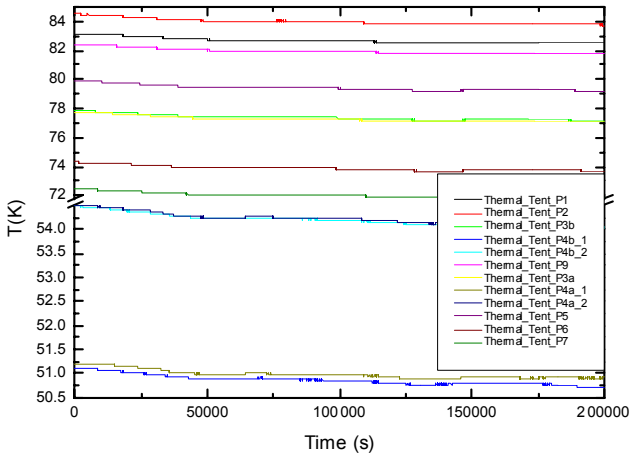

FIG. 18 THERMAL TENT SENSORS DURING SET 2

5.3 SET 3 WARM-UP OF SKY LOAD

The third set of data is representative of the transition between Sets 2 and 1.

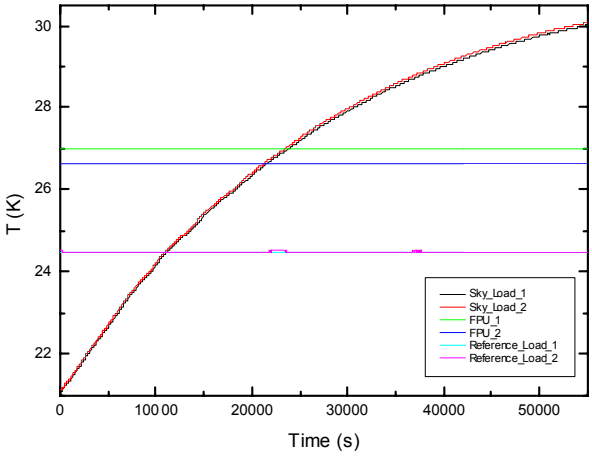

FIG. 19 SET 3 COMPLETE ACQUISITION

Opening the heat switch, the Sky Load is disconnected from 20K cooler and its temperature rises under the effect of radiative coupling with the thermal tent environment.

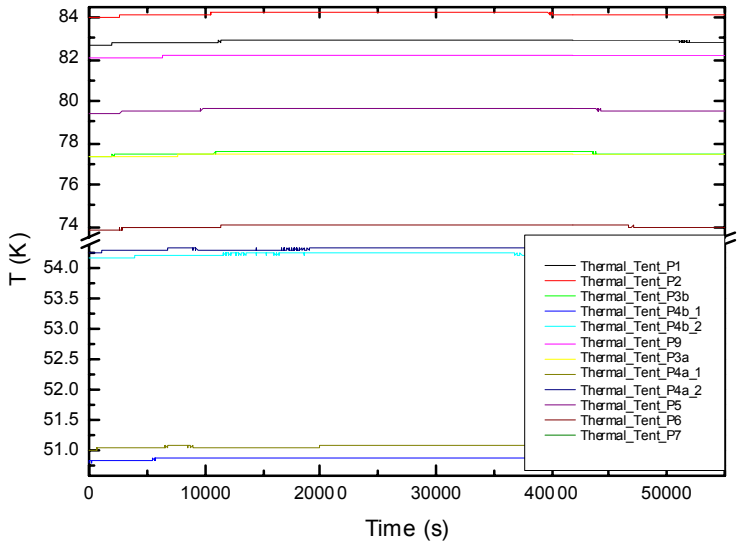

FIG. 20 THERMAL TENT SENSORS DURING SET 3

While the controlled FPU and Ref Load stages are efficiently controlled, the thermal tent shows a quick temperature rise, before restarting a modulated behaviour.

	Mean (K)	STD (K)	Min (K)	Max (K)	Ripple (K)
BEU_1	300.172	0.209	299.807	300.464	0.657
BEU_2	293.326	0.013	293.298	293.369	0.071
VG1_1	166.200	0.009	166.172	166.230	0.058
VG1_2	158.783	0.024	158.709	158.850	0.141
VG2_1	106.200	0.011	106.156	106.255	0.099
VG2_2	105.005	0.018	104.934	105.056	0.121
TT_P1	82.871	0.050	82.715	82.914	0.199
TT_P2	84.182	0.049	84.031	84.239	0.208
TTP32	77.525	0.045	77.380	77.568	0.188
TTP41	50.874	0.013	50.824	50.893	0.069
TTP42	54.242	0.018	54.179	54.265	0.086
TT_P9	82.193	0.043	82.054	82.233	0.179
TTP31	77.453	0.048	77.301	77.496	0.195
TT_41	51.076	0.018	51.030	51.103	0.073
TT_42	54.344	0.019	54.288	54.371	0.083
TTP51	79.589	0.049	79.436	79.636	0.201
TT_P6	74.013	0.049	73.865	74.057	0.192
TT_P7	72.173	0.044	72.031	72.214	0.183
SFt_1	24.862	0.008	24.849	24.883	0.035
SFt_2	24.925	0.007	24.913	24.944	0.031
SS_FI	84.552	0.009	84.540	84.569	0.029
VG3_1	21.549	0.087	21.502	22.411	0.908
VG3_2	58.000	0.003	57.992	58.009	0.017
Sky_1	26.782	2.392	21.365	29.802	8.438
Sky_2	26.844	2.398	21.412	29.870	8.458
FPU_1	27.002	0.010	26.984	27.022	0.038
FPU_2	26.636	0.009	26.617	26.655	0.038
Ref_1	24.500	0.004	24.477	24.506	0.029
Ref_2	24.505	0.004	24.482	24.511	0.029

TABLE 6 COMPLETE STATISTICS ON SET 3

5.4 STABILITY OF DATA

Taking into account thermalization time and noisy subsets, it is possible to conclude that the optimal data for calibration data analysis are

- from 18.00 hrs. of July 19th until 08.00 hrs. of July 21st for Set1
- from the beginning of Set2 until 11.30 hrs. of July 25th

A limited subset of acquisition data is not compliant with the nominal time sampling of 30 s (see Fig. 2); a detailed analysis would be required to verify their impact on the feedback-based temperature control, in order to increase thermal stability in future activity.

6 Conclusions

We presented a preliminary study about the global cryo chamber behaviour in order to understand the mutual interaction of the different temperature stages and their impact on the facility performance. These results could be used as a starting point for a more refined analysis aimed at the optimization of the system in consideration of the future test campaigns.
Radiative power from thermal tent seems to overload the 20 K stages of the chamber. In particular, the radiative coupling between the environment and the sky load reduces the amount of temperature steps available to the load itself, limiting the measurement range during the LFI calibration tests. The minimization of the heat load from the thermal tent to the 20K cooler would also allow the FPU and the Ref Load to reach temperatures closer to the nominal 20 K.
It is therefore of fundamental importance that the FPU, the Sky Load and the Reference Load, are thermally independent. The minimization of the thermal coupling that this analysis has evidenced, should be the first objective of the next efforts needed to improve the cryofacility performance for the LFI FM test campaign.
The correlation between BEU_2 and FPU temperatures would be better studied if data without FPU temperature control were available. The data analyzed do not allow to distinguish if this strong correlation is simply an algorithm effect or the consequence of a relevant thermal link.
In conclusion, the results of this preliminary analysis emphasize the need for a more detailed study on the behaviour of the LFI RAA cryofacility. This effort should be based on a series of specific blank tests dedicated, on the one hand, to carefully evaluate the performance of the chamber while providing, on the other hand, possible solutions to reach the required performance. From what concerns the hardware, this more detailed analysis will mainly require an increased number of thermal sensors to characterize the cryofacility during the blank tests.